Higuchi et al., http://www.jcb.org/cgi/content/full/jcb.201307164/DC1

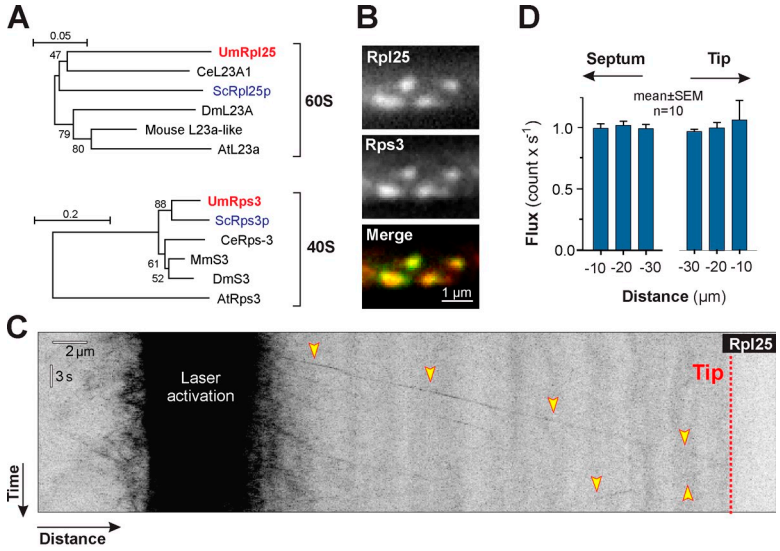

Figure S1. **Characteristics of ribosome motility.** (A) Rpl25 and Rps3 from *U. maydis* (in red) with homologues in other species. The homologue in budding yeast is indicated in blue. Um, *U. maydis*; Ce, *Caenorhabditis elegans*; Sc, *S. cerevisiae*; Mm, *M. musculus*; Dm, *D. melanogaster*; At, *Arabidopsis thaliana*. For accession numbers see Materials and methods. (B) Colocalization of the small ribosomal subunit protein Rps3 and the large ribosomal subunit protein Rpl25. Note that both proteins were tagged by integrating triple mCherry (Rps3) or single GFP (Rpl25) into the native gene loci. This did not cause any detectable phenotype, which indicates that the fusion proteins are functional. Note that all Rpl25-GFP and Rps3-mCherry$_3$ signals colocalize with each other (n = 114 signals from 10 cells). (C) Kymograph showing motility of Rpl25-paGFP–labeled ribosomal subunits (arrowheads) after activation with a 405-nm laser pulse. The growing cell end is indicated by "Tip" and the red dotted line. The image is contrast inverted. (D) Anterograde flux behind the tip and the septum of the cell. All results are given as mean ± SEM (error bars); n = 10 from a single representative experiment. Note that there is no significant difference between all mean values (one-way ANOVA testing, P = 0.9743).

THE JOURNAL OF CELL BIOLOGY

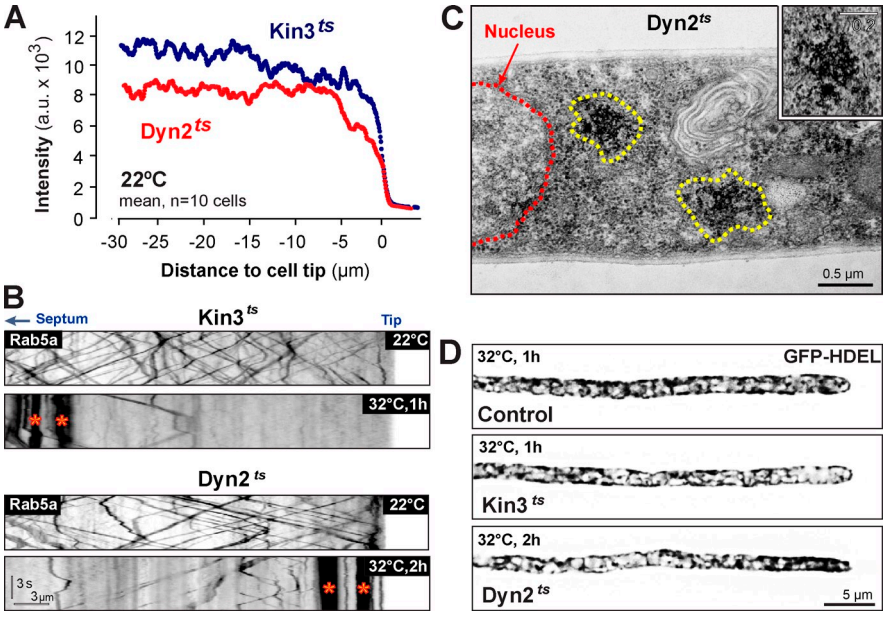

Figure S2. **EE motility, ribosome and ER distribution in mutants.** (A) Fluorescence intensity profiles of Rpl25-GFP along the length of hyphal cells of temperature-sensitive kinesin-3 (Kin3^{ts}) and dynein (Dyn2^{ts}) mutants at a permissive temperature (22°C). Each data point represents the mean value of measurements in 10 cells from a single representative experiment. (B) Kymographs showing motility of EEs labeled with GFP-Rab5a in temperature-sensitive kinesin-3 (Kin3^{ts}) and dynein (Dyn2^{ts}) mutants at permissive (22°C) and restrictive (32°C) temperatures. A shift to the restrictive condition inactivates the mutant motor proteins, resulting in an imbalance of transport that causes clustering of the organelles (EE accumulation is indicated by asterisks). As a consequence, the number of moving EEs is severely reduced. Images are contrast inverted. (C) Electron micrographs showing ribosome clusters (yellow dotted line and insets) in temperature-sensitive dynein mutants (Dyn2^{ts}) after 2 h at 32°C. Ribosome clusters were found near the centrally located nucleus (red dotted line). (D) ER organization in motor mutants at restrictive conditions. The ER was labeled with GFP-HDEL (Wedlich-Söldner et al., 2002) in wild-type cells (Control), temperature-sensitive kinesin-3 (Kin3^{ts}), and dynein (Dyn2^{ts}) mutants. Images are contrast inverted and brightness, contrast, and gamma settings were adjusted.

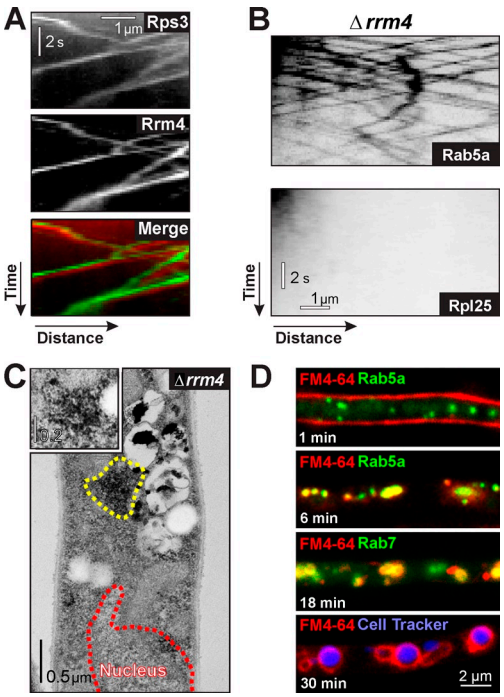

Figure S3. **The role of Rrm4 in ribosome motility and visualization of the endocytic pathway with FM4-64.** (A) Colocalization of the small ribosomal subunit, labeled with Rps3-mCherry$_3$, and the RNA-binding protein Rrm4 with GFP. (B) Kymographs showing motility of EEs (Rab5a) and ribosomes (Rpl25) in null mutants of *rrm4* in a photobleached region. Images are contrast inverted and brightness, contrast, and gamma settings were adjusted. (C) Electron micrographs showing ribosome clusters (yellow dotted line and insets) in *rrm4*-null mutants (Δ*rrm4*). Ribosome clusters were found near the centrally located nucleus (red dotted line). Bar in inset, 0.2 µm. (D) The endocytic pathway in hyphal cells of *U. maydis*, visualized with the endocytic marker dye FM4-64. Rab5a, fusion protein of GFP and the Rab5-like GTPase Rab5a (Fuchs et al., 2006); Rab7, fusion protein of GFP and the Rab7-like GTPase. The vacuolar lumen was stained with Cell Tracker Blue CMAC.

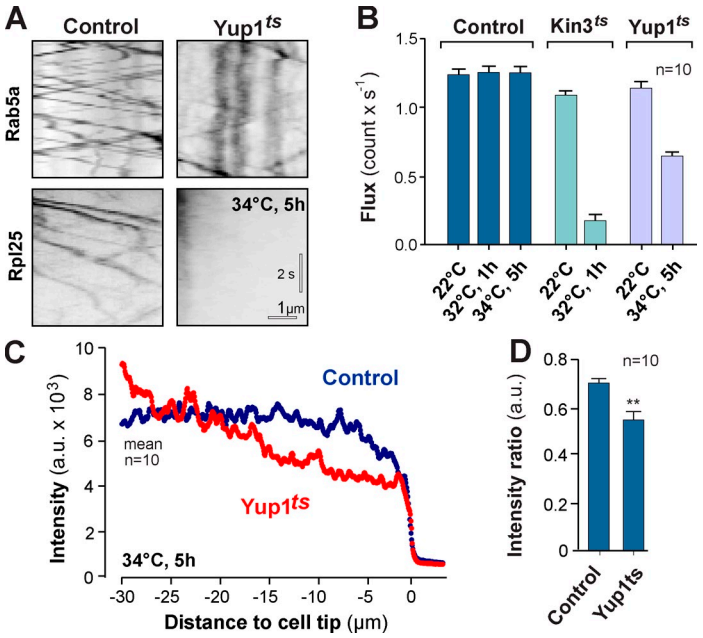

Figure S4. **Ribosome motility and distribution in EE-reduced Yup1^{ts} mutants.** (A) Motility of Rab5-positive EEs and Rpl25-GFP–labeled large ribosomal subunits in control cells (Control) and *yup1*^{ts} mutants (Yup1^{ts}) after 5 h at 34°C. Inactivation of the t-SNARE Yup1^{ts} reduces the number of EEs and affects ribosome motility. Images are contrast inverted and brightness, contrast, and gamma settings were adjusted. (B) Bar chart showing EE flux in control and temperature-sensitive kinesin-3 (Kin3^{ts}) and *yup1* mutants (Yup1^{ts}) at permissive and restrictive temperatures. Results are given as mean ± SEM (error bars); *n* = 10 cells from 1–3 experiments. (C) Fluorescence intensity profiles of Rpl25-GFP along the length of hyphal cells in control cells (Control) and *yup1*^{ts} mutants (Yup1^{ts}) after 5 h at 34°C. Note that the effect on ribosome distribution was mild, which is most likely due to residual EE motility in Yup1^{ts} mutants. Each data point represents the mean value; *n* = 10 cells from a single representative experiment. (D) Bar chart showing the ratio of Rpl25-GFP fluorescence at the tip (5–10 µm) divided by the fluorescent intensity near the nucleus (25–30 µm). **, statistically significant difference at $P < 0.001$. Results are given as mean ± SEM (error bars); *n* = 10 cells from single representative experiments.

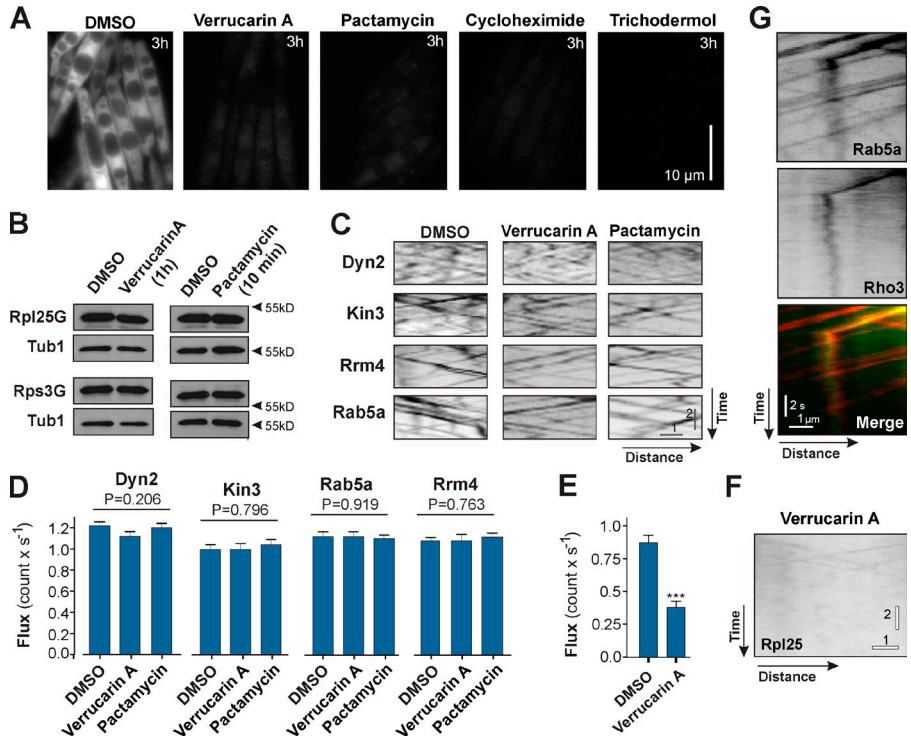

Figure S5. **Effect of translation inhibitors on protein expression and motility of motors, Rrm4, and EEs.** (A) Expression of cytoplasmic GFP from the inducible *crg* promoter after 3 h in inductive medium. Strong expression was seen in the presence of the solvent DMSO, whereas formation of new protein was abolished when translation was inhibited by 10 µg/ml verrucarin A, 100 µM pactamycin, 100 µg/ml cycloheximide, and 100 µg/ml trichodermol for 3 h. This indicates that all inhibitors affect translation in *U. maydis*. (B) Western blots showing Rpl25-GFP and Rps3-GFP in extracts of cells that were treated with the solvent DMSO and the translation initiation inhibitors verrucarin A (10 µg/ml, 1 h min) and pactamycin (100 µM, 10 min). The inhibitors had no obvious effect on the cellular amount of Rpl25-GFP or Rps3-GFP. Note that this is most likely due to the existing proteins, as both inhibitors repress the formation of new protein (see A). (C) Kymographs showing motility of GFP-labeled dynein (Dyn2), kinesin-3 (Kin3), Rrm4, and EEs (Rab5a) in the presence of DMSO, and the translation initiation inhibitors verrucarin A (10 µg/ml, 1 h) and pactamycin (100 µM, 10 min). The inhibitors do not affect the intracellular motility of motors, Rrm4, or EEs. Images are contrast inverted. Bars, 2 s and 1 µm. (D) Anterograde motility of the dynein heavy chain protein GFP_3-Dyn2 (Dyn2), the kinesin-3 motor Kin3-GFP (Kin3), the small GTPase GFP-Rab5a (Rab5a), and the RNA-binding protein Rrm4-GFP (Rrm4). Results of one-way ANOVA testing are indicated above the bars. Short-term treatment of translation initiation inhibitors did not affect the flux of these proteins (also see C). Results are given as mean ± SEM (error bars); n = 10 cells from 1–3 experiments. (E) Bar chart showing the frequency of ribosome motility in the presence of verrucarin A. Results are given as mean ± SEM (error bars); n = 20 cells from single representative experiments. ***, statistical significance at $P < 0.0001$ using a Student's t test. (F) Kymograph showing motility of ribosomes (Rpl25-GFP) in the presence of the translation initiation inhibitor verrucarin A. Only faint Rpl25-GFP signals are visible, and their motility is reduced. Bars, 2 s and 1 µm. Images are contrast inverted and brightness, contrast, and gamma settings were adjusted. See Video 7. (G) Kymographs showing motility and pausing of GFP_3-Rho3 and an EE, labeled with mCherry-Rab5a. Images are contrast inverted, and brightness, contrast, and gamma settings were adjusted.

Table S1. **Experimental usage of strains**

Strain name	Type of experiment	Figure or video
AB33nRFP	Analyses of shape of hypha and localization of nucleus	Fig. 1 A
AB33	Analyses of ribosome distribution and morphological phenotype	Figs. 1 B and 6
AB33R25G	Analyses of ribosome motility and distribution	Figs. 1 (C and D), 2 E, 3 (B and D), 4 (A, B, and D), 7 (B, E, and F), 8 (A and E), S1 D, S4 (A–D), S5 (B, E, and F), and Videos 6 and 7
AB33R3Ch$_3$	Ribosome distribution analysis	Fig. 1 C
AB33R25paG	Diffusion analysis of Rpl25-paGFP	Figs. 2 (A–D), 7 (H, J, and K), and S1 C
AB33paG$_2$	Diffusion analysis of 2×paGFP	Fig. 2 D
AB33R3Ch$_3$_R25G	Colocalization of Rps3 and Rpl25	Fig. 3 A, Fig. S1 B, and Video 1
AB33ΔKin3_R25G	Ribosome motility analysis	Fig. 3 (C and D)
AB5Dyn2^{ts}_R25G	Analyses of ribosome motility and distribution	Figs. 3 (C and D), 4 (A, B, and D), and S2 (A and C)
AB33ΔKin3_Kin3^{ts}_R25G	Ribosome distribution analysis	Figs. 4 (A–D) and S2 A
AB33R25G_ChRab5a_ΔRrm4	Ribosome and early endosome motility analysis	Figs. 4 B, 6, and S3 (B and C)
AB33EG	ER distribution analysis	Figs. 4 E and S2 D
AB33ΔKin3_EG_Kin3^{ts}	ER distribution analysis	Figs. 4 E and S2 D
AB5Dyn2^{ts}_EG	ER distribution analysis	Figs. 4 E and S2 D
AB33R25G_ChRab5a	Ribosome and early endosome motility analysis	Figs. 5 A, 7 (C and D), and 8 (B and F), and Videos 5, 7, and 8
AB33GRab5a	Early endosome motility analysis	Figs. 5 B, 8 A, S3 D, S4 B, and S5 (C and D)
AB33ChRab5a_PXG	Colocalization of early endosome and PX domain	Fig. 5 C
AB33ChRab5a_GRab4	Colocalization of Rab5a and Rab4	Fig. 5 E
AB33ChRab5a_GRab7	Colocalization of Rab5a and Rab7	Fig. 5 (F and G)
AB33ΔKin3	Morphological phenotype analysis	Fig. 6
FB2N107G	Internal calibration standard of GFP intensity analysis	Fig. 7 A
AB33ChRab5a_G$_3$Rho3	Colocalization of early endosome and Rho3	Figs. 7 G and S5 G
AB33Rrm4G	Rrm4 motility analysis	Figs. 8 A and S5 (C and D)
AB33ChRab5a_Rrm4G	Off-loading of Rrm4 from early endosome	Figs. 8 C and S3 A
AB33R3Ch$_3$_Rrm4G	Colocalization of Rps3 and Rrm4	Fig. 8 D and Video 4
AB33ΔKin3_Kin3^{ts}_GRab5a	Early endosome motility analysis	Figs. S2 B and S4 B
AB5Dyn2^{ts}_GRab5a	Early endosome motility analysis	Fig. S2 B
AB33GRab7	Colocalization of Rab7 and FM4-64	Fig. S3 D
AB33Yup1^{ts}_GRab5a	Early endosome motility analysis	Fig. S4 (A and B)
AB33Yup1^{ts}_R25G	Analyses of ribosome distribution and motility	Fig. S4 (A, C, and D)
FB2N107R_cG	Cytoplasmic GFP expression analysis	Fig. S5 A
AB33R3G	Expression amount analysis of Rps3	Fig. S5 B
AB33G$_3$Dyn2	Dynein motility analysis	Fig. S5 (C and D)
AB33Kin3G	Kinesin-3 motility analysis	Fig. S5 (C and D)
AB33R25G_ChT	Analysis of ribosome motility along microtubule	Video 2

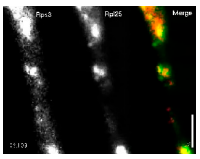

Video 1. **Bidirectional motility of ribosomes.** GFP was fused to the C terminus of the endogenous Rpl25, which labels the large ribosomal subunit (green), and a triple mCherry tag was fused to the C terminus of the small ribosomal subunit protein Rps3 (red). Both subunits travel together, which suggests that entire ribosomes undergo directed motion. Images were analyzed by epifluorescence microscopy using a laser-based inverted microscope (IX81; Olympus; equipped with a VS-LMS4 Laser Merge System; Visitron). Time is given in seconds and milliseconds. Bar, 2 µm.

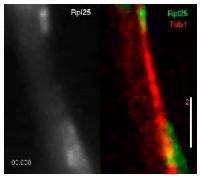

Video 2. **Ribosome motility along microtubule.** The large ribosomal subunit was labeled with Rpl25-GFP (Rpl25; green), and an MT track was labeled by mCherry–α-tubulin (Tub1; red). Images were analyzed by epifluorescence microscopy using a laser-based inverted microscope (IX81; Olympus; equipped with a VS-LMS4 Laser Merge System; Visitron). Time is given in seconds and milliseconds. Bar, 2 µm.

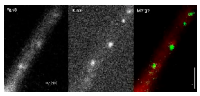

Video 3. **Colocalization of ribosomes and kinesin-3.** The small ribosomal subunit was labeled with Rps3-mCherry$_3$ (Rps3; red), and the motor was C-terminally fused to GFP (Kin3; green). Images were analyzed by epifluorescence microscopy using a laser-based inverted microscope (IX81; Olympus; equipped with a VS-LMS4 Laser Merge System; Visitron). Time is given in seconds and milliseconds. Bar, 2 µm.

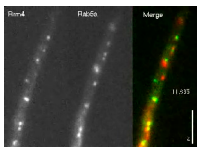

Video 4. **Colocalization of the RNA-binding protein Rrm4 and EEs.** The endogenous copy of Rrm4 was C-terminally fused to GFP (Rrm4; green) and coexpressed with the endosomal small GTPase Rab5a, N-terminally fused to mCherry (Rab5a; red). Note that the video confirms previous work by Baumann et al., 2012. Images were analyzed by epifluorescence microscopy using a laser-based inverted microscope (IX81; Olympus; equipped with a VS-LMS4 Laser Merge System; Visitron). Time is given in seconds and milliseconds. Bar, 4 µm.

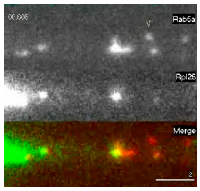

Video 5. **Colocalization of ribosomes and EEs.** The large ribosomal subunit was marked by Rpl25-GFP (Rpl25; green), and the organelles were labeled by mCherry-Rab5a (Rab5a; red). The cell was photobleached to reduce cytoplasmic background. Note that some EEs do not carry ribosomes (arrowheads). Images were analyzed by epifluorescence microscopy using a laser-based inverted microscope (IX81; Olympus; equipped with a VS-LMS4 Laser Merge System; Visitron). Time is given in seconds and milliseconds. Bar, 2 µm.

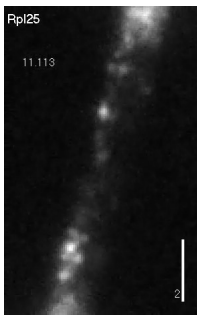

Video 6. **Bidirectional motility of Rpl25-GFP signals with variable intensity.** The endogenous copy of Rpl25 is tagged with GFP. The fluorescent intensity of the resulting Rpl25-GFP protein is directly proportional to the number of this ribosomal protein. Note that a single Rpl25-GFP would not be visible due to limitations in microscopic light sensing. In addition, the Rpl25-GFP signal intensity varies remarkably, which suggests that variable numbers of ribosomes bind to individual endosomes. Images were analyzed by epifluorescence microscopy using a laser-based inverted microscope (IX81; Olympus; equipped with a VS-LMS4 Laser Merge System; Visitron). Time is given in seconds and milliseconds. Bar, 2 µm.

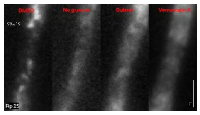

Video 7. **Ribosome under stress conditions and in the presence of translation inhibitors.** In the presence of the solvent DMSO, ribosomes, labeled with the large ribosomal subunit protein Rpl25-GFP (Rpl25), show normal bidirectional motility. Depletion of glucose for 10 min (No glucose) and the presence of 1% butanol for 10 min affect polysome formation in *Saccharomyces cerevisiae* (Ashe et al., 2000, 2001). When applied to *U. maydis* cells, almost all ribosome motility stopped. Inhibition of translation initiation by verrucarin A (10 µg/ml, 1 h) drastically impaired ribosome motility. Note that the effectiveness and toxicity of the inhibitor was tested (see Fig. S5 A). Images were analyzed by epifluorescence microscopy using a laser-based inverted microscope (IX81; Olympus; equipped with a VS-LMS4 Laser Merge System; Visitron). Time is given in seconds and milliseconds. Bar, 2 µm.

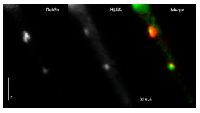

Video 8. **Off-loading of ribosomes from anterograde moving EEs.** EEs labeled with mCherry-Rab5a (Rab5a, red) move into the photobleached apical region of the cell. They carry ribosomes, marked by Rpl25-GFP (Rpl25, green), which occasionally detach from the moving organelles (arrowheads). Note that the intensity of the Rpl25-GFP signal suggests that numerous ribosomes are deposited together, probably as part of a polysome. Images were analyzed by epifluorescence microscopy using a laser-based inverted microscope (IX81; Olympus; equipped with a VS-LMS4 Laser Merge System; Visitron). Time is given in seconds and milliseconds. Bar, 2 µm.

References

Ashe, M.P., S.K. De Long, and A.B. Sachs. 2000. Glucose depletion rapidly inhibits translation initiation in yeast. *Mol. Biol. Cell*. 11:833–848. http://dx.doi.org/10.1091/mbc.11.3.833

Ashe, M.P., J.W. Slaven, S.K. De Long, S. Ibrahimo, and A.B. Sachs. 2001. A novel eIF2B-dependent mechanism of translational control in yeast as a response to fusel alcohols. *EMBO J.* 20:6464–6474. http://dx.doi.org/10.1093/emboj/20.22.6464

Baumann, S., T. Pohlmann, M. Jungbluth, A. Brachmann, and M. Feldbrügge. 2012. Kinesin-3 and dynein mediate microtubule-dependent co-transport of mRNPs and endosomes. *J. Cell Sci.* 125:2740–2752. http://dx.doi.org/10.1242/jcs.101212

Fuchs, U., G. Hause, I. Schuchardt, and G. Steinberg. 2006. Endocytosis is essential for pathogenic development in the corn smut fungus *Ustilago maydis*. *Plant Cell*. 18:2066–2081. http://dx.doi.org/10.1105/tpc.105.039388

Lenz, J.H., I. Schuchardt, A. Straube, and G. Steinberg. 2006. A dynein loading zone for retrograde endosome motility at microtubule plus-ends. *EMBO J.* 25:2275–2286. http://dx.doi.org/10.1038/sj.emboj.7601119

Schuster, M., S. Kilaru, P. Ashwin, C. Lin, N.J. Severs, and G. Steinberg. 2011a. Controlled and stochastic retention concentrates dynein at microtubule ends to keep endosomes on track. *EMBO J.* 30:652–664. http://dx.doi.org/10.1038/emboj.2010.360

Schuster, M., S. Kilaru, G. Fink, J. Collemare, Y. Roger, and G. Steinberg. 2011b. Kinesin-3 and dynein cooperate in long-range retrograde endosome motility along a nonuniform microtubule array. *Mol. Biol. Cell*. 22:3645–3657. http://dx.doi.org/10.1091/mbc.E11-03-0217

Schuster, M., R. Lipowsky, M.A. Assmann, P. Lenz, and G. Steinberg. 2011c. Transient binding of dynein controls bidirectional long-range motility of early endosomes. *Proc. Natl. Acad. Sci. USA*. 108:3618–3623. http://dx.doi.org/10.1073/pnas.1015839108

Steinberg, G., M. Schuster, U. Theisen, S. Kilaru, A. Forge, and M. Martin-Urdiroz. 2012. Motor-driven motility of fungal nuclear pores organizes chromosomes and fosters nucleocytoplasmic transport. *J. Cell Biol.* 198:343–355. http://dx.doi.org/10.1083/jcb.201201087

Wedlich-Söldner, R., I. Schulz, A. Straube, and G. Steinberg. 2002. Dynein supports motility of endoplasmic reticulum in the fungus *Ustilago maydis*. *Mol. Biol. Cell*. 13:965–977. http://dx.doi.org/10.1091/mbc.01-10-0475